CrossMark

Solid–Liquid Phase Equilibria, Molecular Interaction and Microstructural Studies on (*N*-(2-ethanol)-*p*-nitro-aniline + *N*-(2-acetoxyethyl)-*p*-nitroaniline) Binary Mixtures

Salim Chelouche[1] · Djalal Trache[1] · Simão P. Pinho[2,3] ·
Kamel Khimeche[1] · Abderrahmane Mezroua[1] · Mokhtar Benziane[4]

Abstract

Differential scanning calorimetry (DSC) is used to investigate the thermal properties of *N*-(2-ethanol)-*p*-nitroaniline + *N*-(2-acetoxyethyl)-*p*-nitroaniline, and their binary systems. The experimental results demonstrate that the studied binary system presents a simple eutectic behavior and the corresponding mole fraction (x_{eu}) of *N*-(2-ethanol)-*p*-nitroaniline at the eutectic point is 0.5486, whereas the temperature (T_{eu}) is found to be equal to 363.6 K. The quality of the solid–liquid equilibria (SLE) data has been checked by thermodynamic consistency tests, presenting good quality factor. The SLE data have been correlated by means of Wilson, NRTL, and UNIQUAC equations. The three models describe satisfactorily the phase diagram as the root-mean-square deviations for the equilibrium temperatures vary from 1.25 K to 2.07 K. Nevertheless, the Wilson model provides the best correlation results. The three equations have also been used to compute excess thermodynamic functions viz. excess Gibbs energy, enthalpy and entropy. The obtained results revealed a sensitive positive deviation to ideality thus demonstrating the nature of the interactions between the compounds forming the mixture. Microstructural studies have been carried out by FTIR, XRD and optical microscopy showing weak molecular interactions for the eutectic mixture.

Extended author information available on the last page of the article

1 Introduction

For military purposes, propellants are commonly used as filling materials to ensure propulsion of rockets and missiles. Since weapon systems are frequently required to be stored under field conditions for a long time and in order to preserve, chemical, thermal, mechanical and ballistic performances, one of the common basic requirements of such materials is high thermal stability under adverse storage conditions [1, 2]. Therefore, issues related to stability have received special consideration while designing, developing, manufacturing and storing these weapon systems containing energetic materials. Weapons must be ready for use at a short notice and must operate reliably as originally designed after prolonged storage.

In the case of nitrate ester-based propellants such as nitrocellulose, nitroguanidine, pentaerythritol tetranitrate (PETN), triethylene glycol dinitrate and 1,2-propylene glycol dinitrate, slow but autocatalytic decomposition of the nitrate ester takes place even at ambient temperatures because of the low bonding energy of the nitric ester group [3–5] to form oxides of nitrogen, mainly nitrogen dioxide and other products that can affect adversely the stability. The consequence of instability could be catastrophic since the inherent instability of nitrate esters-based propellant leads to self-ignition. Likewise, the effects of nitrate esters decomposition may include alterations in the chemical, physical and ballistic properties [6, 7].

This phenomenon is limited by the addition of a stabilizer to these propellants, and thus, the stability and shelf-life of these propellants increases without affecting their manufacturing processes and properties. These additives cannot prevent the decomposition but are able to inhibit it and avoid the catalytic effect caused by the decomposition products such as NO, NO_2, HNO_2 and HNO_3.

The action of the common stabilizers can be explained by their ability to establish chemical bonds with the decomposition products which are evolved during storage. Several chemicals have been tested for use as stabilizers in nitrate ester-based propellant. The conventional stabilizers employed belong to (a) aromatic amines such as diphenylamine (DPA), 2-nitro-diphenylamine (2-NDPA) and *p*-nitro-*N*-ethylaniline and (b) urea compounds such as *N*,*N'*-diethyl-*N*,*N'*-diphenylurea (C1), *N*,*N'*-dimethyl-*N*,*N'*-diphenylurea (C2) and *N*-methyl *N'*,*N'*-diphenylurea (AKII) [2].

Any potential new stabilizer must fulfill a number of essential requirements, in order to gain widespread acceptance as a potential propellant's stabilizer. Several chemical substances have been developed to fulfill the required characteristics of efficient stabilizers such as triphenylamine, ketones, phenols, natural products, malonanilides, polymers, ionic liquids, zeolites and *N*-methyl-*p*-nitroaniline derivatives [2].

Recently, the stability of nitrate ester-based propellants has garnered a tremendous level of attention from the research community, what is revealed by the increasing number of scientific publications in the field over the two past decades. Several research works dealing with the investigation of the stabilizing effect of various organic and inorganic substances have been published, and this area of research is still of significant interest worldwide and studies on new stabilizers continue to be conducted.

Among different materials, eutectic mixtures are of potential interest in the field of technology and material science [8, 9]. Organic eutectics may act as a blend material, and hence, their investigation for possible use in the synthesis of nitrate ester-based propellants is important and should be done in detail. The thermodynamic properties and structural details of these mixtures are very scarce. Moreover, and despite the fact that the behavior of conventional stabilizers has been the subject of numerous investigations, relatively little is known about the nature of the component interactions occurred in a propellant containing a mixture of two organic stabilizers. In this paper, we perform phase equilibria, molecular interaction and microstructure studies by means of DSC, FTIR, XRD and optical microscopy, for a binary mixture of organic stabilizers, that is *N*-(2-ethanol)-*p*-nitroaniline + *N*-(2-acetoxyethyl)-*p*-nitroaniline. In particular, SLE data have been correlated by means of Wilson, NRTL and UNIQUAC equations, which were also employed to compute excess thermodynamic functions, to better unveil the interactions occurred between the constituents of the studied stabilizer.

2 Experimental and Methods

2.1 Materials

The chemical structure of the compounds used to prepare our system is given in Fig. 1. *N*-(2-ethanol)-*p*-nitroaniline (ENA) and *N*-(2-acetoxyethyl)-*p*-nitroaniline (ANA) were synthesized and purified following the method indicated by Gibson [10]. Their purities were checked by DSC analysis and FTIR, and was confirmed by high-performance liquid chromatography (SHIMADZU LC10-AD) and evaluated to be higher than 98 (wt%). Figure S1 shown in the supplementary material presents the DSC curves of the two pure components, while Table 1 compiles their source and purity.

Their melting temperatures and fusion enthalpies were measured by DSC. Table 2 lists the obtained results and the comparison for melting temperatures with the avail-
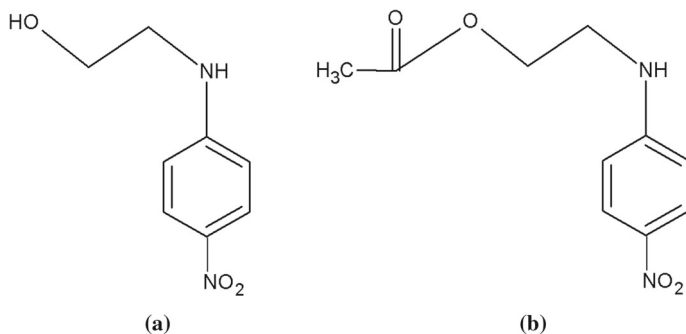

Fig. 1 Chemical structure of the studied compounds: (a) *N*-(2-ethanol)-*p*-nitroaniline (ENA); (b) *N*-(2-acetoxyethyl)-*p*-nitroaniline (ANA)

Table 1 Source, purification method and final mass fraction purity of the studied compounds

Chemical name	Source	Initial mass fraction purity	Purification method	Final mass fraction purity	Analysis method
N-(2-ethanol)-p-nitroaniline (ENA)	Synthesis in our laboratory	–	Repeated crystallization + Filtration	>0.98	DSC[a] FTIR[b] HPLC[c]
N-(2-acetoxyethyl)-p-nitroaniline (ANA)	Synthesis in our laboratory	–	Repeated crystallization + Filtration	> 0.98	DSC[a] FTIR[b] HPLC[c]

[a]Differential scanning calorimeter
[b]Fourier transformed infrared
[c]High-performance liquid chromatography

Table 2 Physical properties of pure compounds: molar volume at density temperature $T_\rho = 298.15$ K ($V^{298.15}$), the fusion temperature (T_{fus}) and the enthalpy of fusion (ΔH_{fus}) in the DSC experiments, at $p = 0.1$ MPa

Compound	$V_M^{298.15}$ (cm^3·mol^{-1})	T_{fus} (K)	ΔH_{fus} (kJ·mol^{-1})
N-(2-ethanol)-p-nitroaniline (ENA)	137.5[a] 138.6[b]	382.1[a] 380.65–383.15 [10]	26.5[a] 29.45 [14] 25.65 [15]
N-(2-acetoxyethyl)-p-nitroaniline (ANA)	169.2[a] 169.4[b] 168.6[c]	387.4[a] 387.0 [12] 388.15–392.15 [10]	20.7[a] 20.8 [12]

Standard uncertainties u are: $u(V) = 0.4$ cm^3·mol^{-1}, $u(T_{fus}) = 0.2$ K, $u(\Delta H_{fus}) = 0.3$ kJ·mol^{-1}, $u(T_\rho) = 0.07$ K, $u_r(p) = 0.05$
[a]This work
[b]Girolami's method [16]
[c]Imerizi's method [16]

able literature data. The knowledge of these physicochemical properties is of great importance for the determination of the activity coefficients as well as for the thermodynamic modeling. Additionally, Table 2 presents also the experimental molar volumes (V_M, cm^3·mol^{-1}), which are calculated according to Eq. 1 [11],

$$V_M = \frac{M}{\rho} \tag{1}$$

where M is the mass molar (g·mol^{-1}) of the pure compound, and ρ its density (g·cm^{-3}) measured at 298.15 K.

2.2 Apparatus and Procedure

Before carrying out the DSC experiments, a series of solid binary mixtures have been first prepared. Considerable caution has been paid in preparing the samples; each mixture is placed in a separate Pyrex glass test tube and kept airtight. The solids are slowly

mixed and heated up to a temperature about 10 °C above the temperature of component presenting higher melting temperature. When the first droplets of liquid appear, rapid and continuous stirring is recommended in order to ensure a good homogeneity of the binary mixture. The mixtures were then allowed to cool down to room temperature. The resulting solid was powdered in a clean agate mortar with a little pressure as possible and dried in desiccators.

The thermal property measurements were carried out by means of a PerkinElmer DSC8000 (PerkinElmer, Inc., 710 Bridgeport Avenue Shelton, CT 06484-4794, USA). DSC device was calibrated with high pure indium and lead and confirmed by analysis with zinc. As indicated in the user's manual device, a cleaning of the measuring equipment is done ahead by heating to 600 °C with an opened sample holder cover and furnaces exposed to air. For each measurement, 4 to 6 mg (Mettler H31 balance, precision 0.0002 g) of the sample is charged to cramped aluminum crucibles, while an empty pan of the same type is employed as a reference.

In order to guarantee homogenization and uniformity of the sample and preventing that thermal histories and polymorphic effects affect the accuracy of the analysis, each sample undergoes first a heating cycle in which it is heated until a temperature 15 K above the melting of the mixture's component presenting the higher melting temperature. At this temperature, the sample is kept for additional 20 min. Afterward, it was cooled down to room temperature and kept in this state for 20 min.

Following, a second heating is performed in a nitrogen atmosphere (2 K·min^{-1}) in the temperature range 320–400 K. This scanning rate is low enough to approach the equilibrium measurement conditions [12, 13] and to increase the accuracy of the enthalpy of fusion calculations. Any further attempt to use a slower heating rate (1 K·min^{-1}) does not influence the quality and the precision of the measured data.

The determination of the enthalpies and temperatures of fusion and the processing of the curves were done with PerkinElmer's Pyris software (PerkinElmer Life and Analytical Science, Chalfont Road, Seer Green, Buckinghamshire, HP9 2FX, UK). Measurement uncertainties were estimated to be 0.0005 for the mole fraction, 0.2 K for the temperature and did not exceed 0.3 kJ·mol^{-1} for the enthalpy of fusion.

Pure component densities were measured using a helium gas pycnometer (Micromeritics, AccuPyc II 1340, Georgia, USA). The volume of the two components is measured by replacing their void space with helium. The density is determined with independent and simultaneous measurements of the mass. The measurements were made three times, where each one consisted of 10 measurement cycles, providing 10 data points. Measurement uncertainties were estimated to be better than 0.003 g·cm^{-3}.

FTIR study is considered to provide information about molecular interactions. For analysis, samples were embedded in KBr pellets and analyzed by using a Shimadzu spectrometer 8400S. The spectra were recorded in transmittance mode in the range of $4000–600 \text{ cm}^{-1}$. 64 scans were co-added to achieve an acceptable signal-to-noise ratio. In all measurements, spectra resolution was maintained at 4 cm^{-1}.

XRD analysis was carried out using a PANalytical X'Pert Pro X'Pert Pro Multi-Purpose Diffractometer with Cu Kα radiation. An X'Celerator detector was used to collect data over an angular range of $10°–30°/2\theta$, with a step size of $0.0170/2\theta$ and a count time of 50.1650 s at each step. The voltage was chosen to be 45 kV with a current of 40 mA. Powdered specimens were prepared for X-ray diffraction analysis using the
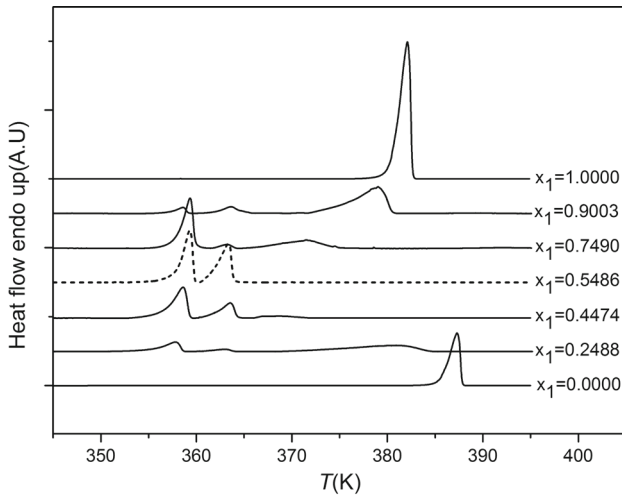
Fig. 2 DSC thermograms of ENA (1) + ANA (2) binary mixtures

PANalytical powder sample preparation Kit and back-loaded into nickel-coated steel sample holders.

The microstructural characterization of the pure components and their eutectic composition has been performed using an optical microscope type "Leica DM 2500 M." The samples were analyzed with the magnification of 50 times. Microstructure inspection is carried out in order to know more about the disposition of the pure compound grains and eventual modifications undergone during the formation of the eutectic. The stabilizers are placed on glass slides in small quantities and then heated until melting. The recrystallization is carried out at ambient temperature.

3 Results and Discussion

3.1 Phase Equilibria

3.1.1 Solid–Liquid Phase Diagram

Some typical DSC curves for the binary system ENA (1) + ANA (2) are plotted in Fig. 2, while Table 3 presents the obtained results.

The DSC curves of pure components exhibit only an endothermic effect, corresponding to the melting phenomenon. A good agreement with the literature data has been observed [10]. For ENA melting enthalpy and both pure compounds molar volume, no experimental data were possible to find, and instead estimating methods were applied [14–16], showing satisfactory coherence with the values measured in this work.

Regarding the mixture thermograms, three melting DSC peaks were observed. The last two peaks were attributed, respectively, to the melting of the eutectic and that of

Table 3 Experimental liquidus temperatures (T) for ENA (1) + ANA (2) system at different ENA mole fractions (x_1) and $p = 0.1$ MPa

x_1	T_2 (K)	T_1 (K)
0.0000	387.4	
0.0536	386.1	
0.1014	385.1	
0.1484	384.2	
0.1991	382.9	
0.2488	380.7	
0.2975	377.9	
0.3509	375.6	
0.4022	372.8	
0.4474	369.5	
0.4997	366.8	
0.5436	364.3	
0.5486	363.6	
0.6005		365.3
0.6487		367.4
0.7025		369.7
0.7490		371.4
0.7994		373.4
0.8487		376.3
0.9003		378.9
0.9476		380.2
1.0000		382.1

Standard uncertainties u are: $u(x) = 0.0005$, $u(T) = 0.2$ K, $u_r(p) = 0.05$

the liquidus line registered at a higher temperature. In addition to those two peaks, a third one was observed for all mixtures at the same temperature, slightly lower than that of the eutectic and assigned to a solid–solid transition. This observed transition which does not appear in the pure compounds (ENA or ANA) may be interpreted as the decomposition of an intermediate solid below the eutectic, such as a peritectoid reaction [17].

The eutectic temperature is observed, at a constant value, unlike that of the mixture melting point, which changes with the composition, so the studied system exhibits a simple eutectic behavior with complete miscibility in the liquid phase and immiscibility in the solid phase.

3.1.2 Eutectic Mixture Mole Fraction and Temperature Determination

From the characteristic Tamman's triangle shape, [18] obtained after a linear regression of the eutectic enthalpy of fusion versus the molar fraction data points (Fig. 3), the eutectic composition of the ENA (1) + ANA (2) system is estimated to be: $x_{1,eu} = 0.5486$.

In order to measure more accurately the eutectic temperature, a mixture has been prepared at a mole fraction defined from Tamman plot and following the same exper-
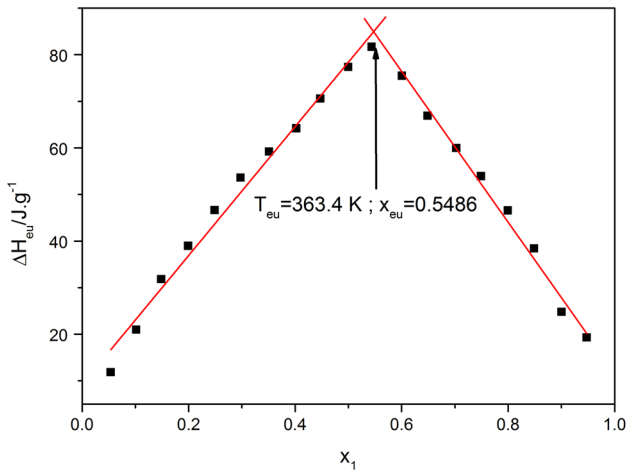
Fig. 3 Tamman plot of the studied binary system ENA (1)+ANA (2)

Table 4 Comparison between the experimental coordinates for the eutectic temperature (T_{eu}) and the mole fraction ($x_{1,eu}$) with calculated values

System	T_{eu} (K)		$x_{1,eu}$	
	Exp.	Cal.	Exp.	Cal.
ENA (1)+ANA (2)	363.6[a]	361.5[c]	0.5486[b]	0.5750[c]
		363.2[d]		0.5818[d]
		365.1[e]		0.5990[e]
		351.4[f]		0.4833[f]

[a]Experimental eutectic temperature uncertainty $u(T_{eu})=0.2$ K
[b]Calculated eutectic molar fraction uncertainty from Tamman plot $u(x_{eu})=0.0179$
[c]Calculated by Wilson
[d]Calculated by NRTL
[e]Calculated by UNIQUAC
[f]Calculated by Ideal model

imental procedure analyzed by DSC. The thermogram corresponding to the eutectic reported in Fig. 2 (dashed line) shows two endothermic peaks (solid–solid transition and eutectic fusion, respectively). The eutectic melting temperature measured is found to be equal to 363.6 K. Likewise, the experimental enthalpy of fusion of the eutectic is evaluated to be equal to 17.3 kJ·mol^{-1}.

The eutectic coordinates are summarized in Table 4. However, the uncertainties associated with the experimental eutectic temperature, molar fraction and melting enthalpy are found to be equal to the experimental errors associated with the measured samples given above. Furthermore, the mole fraction uncertainty estimated from the Tamman plot is found to be less than 0.0179.

Table 5 Quality factor value for the studied system

ENA + ANA	Exp. (pure)	From SLE	Δ	Quality factors		Q_{SLE}
Tf1/K	382.1	381.7	0.4	F1	1 * 0.25	0.780
Tf2/K	387.4	387.1	0.3	F2	1 * 0.25	
Slope 1	0.0218	0.0234	0.073	F3	1 * 0.25	
Slope 2	0.0167	0.0451	1.700	F4	0.118 * 0.25	

The studied system has a high eutectic temperature, and thus, it can be introduced into propellant formulations without altering their thermal stability, material structure integrity and the desired chemical, mechanical and ballistic characteristics [2].

3.1.3 Consistency Tests

Consistency tests for all types of phase equilibria were proposed by Kang et al. [19]. The procedures proposed are essential for the validation of the experimental data and the development of high-quality prediction and correlation models. Solid–liquid equilibrium experimental data of the investigated binary mixture, together with relevant properties of pure compounds, are used to verify the consistency of the data measured in this work. A quality factor Q_{SLE} ranging between 0 and 1 is computed based on the differences between the melting temperature and the enthalpy estimated from binary solubility data and the pure component property values. The detailed procedure can be found in the work by Kang et al. [19]. The obtained results for Q_{SLE} are reported in Table 5, where the good quality of the measured data is confirmed since the global quality factor of the studied system is found to be equal to 0.780.

3.1.4 Application of Semi-empirical Models

The mixture's components are not miscible in the solid phase and completely miscible in the liquid phase. Therefore, the activity coefficient (γ_1) of the component, in the liquid phase, can be calculated according to Eq. 2 [5, 20, 21].

$$\ln x_1 \gamma_1 = -\frac{\Delta_{fus} H_1}{R}\left(\frac{1}{T} - \frac{1}{T_{fus,1}}\right) + \frac{\Delta_{fus} C_{p,1}}{R}\left(\frac{T_{fus,1} - T}{T} + \ln \frac{T}{T_{fus,1}}\right) \quad (2)$$

where x_1, $\Delta_{fus} H_1$, $\Delta_{fus} C_{p,1}$ and $T_{fus,1}$ stand, respectively, for the mole fraction, the enthalpy of fusion, the difference in the heat capacity between liquid and solid states at the melting temperature and melting temperature of pure solute 1, and T is equilibrium temperature of the binary system. As suggested by Prausnitz et al. [22], the first term on the right hand side of Eq. 2 is dominant. The heat capacity term is generally small enough and not known, and then is usually neglected when compared to the other terms. Because of the unavailability of C_p values of the pure components in both liquid and solid states, some tests were performed. In fact, testing different values for the heat capacity change of ANA, which presents the lower fusion entropy,

even when this value is as high as 50 J·mol^{-1}·K^{-1}, the importance of the second term in the right side of Eq. 2 is always lower than 2.95%, guaranteeing the validity of the simplification.

The deviation from ideal behavior and the types of interactions governing the system can be better explained by means of excess thermodynamic functions, namely excess Gibbs energy (G^E), excess enthalpy (H^E) and excess entropy (S^E) [23–25]. These functions give a more quantitative idea about the nature of molecular interactions and are expressed as the difference between the thermodynamic functions of a real system and the ideal one at the same temperature and pressure. In this study, three equations were used to calculate the solute activity coefficients and to correlate the SLE data: Wilson, NRTL and the UNIQUAC models.

The unknown parameters of models were found by minimizing the objective function F_0 using simplex method [26]:

$$F_0 = \sum_{i=1}^{n} \left\{ T_i^{exp} - T_i^{cal}(x_{1i}, A_1, A_2) \right\}^2 \tag{3}$$

where n is the number of experimental points, T_i^{exp} and T_i^{cal} are, respectively, the experimental and calculated equilibrium temperatures at a given concentration x_{1i}, and A_1 and A_2 are the two adjustable parameters of each correlation model.

The root-mean-square deviation of temperature was defined as:

$$\sigma_T = \left[\sum_{i=1}^{n} \frac{(T_i^{exp} - T_i^{cal})^2}{n - m} \right]^{1/2} \tag{4}$$

where m is the number of adjustable parameters which is equal to 2 in our case. The NRTL equation contains three parameters, but the reduction of experimental data for a large number of binary systems indicates that the non-randomness parameter α_{12} varies from about 0.20 to 0.47 [22]. A typical choice is $\alpha_{12} = 0.3$ [12, 20, 22] here adapted. Furthermore, the pure component structural parameters r (volume parameter) and q (surface parameter) in the UNIQUAC equations were calculated according to the procedure suggested by Hofman and Nagata [27].

The estimated parameters and corresponding root-mean-square deviations are summarized in Table 6. Figure 4 provides a comparison between the experimental data and the correlation results as well as with the liquidus line assuming ideality. The three models calculate equilibrium temperatures satisfactory with standard deviations for Wilson, NRTL and UNIQUAC of 1.25, 1.80 and 2.07 K, respectively. As shown in Table 4, the deviation between the experimental and calculated values of T_{eu} and x_{eu} is more important in the case of ideal solubility. However, eutectic coordinates calculated by the three equations are relatively close to the values found using the Tamman plot.

Table 6 Correlation of the (solid + liquid) data of the binary mixture by means of Wilson, NRTL and UNIQUAC equations: values of parameters and deviations

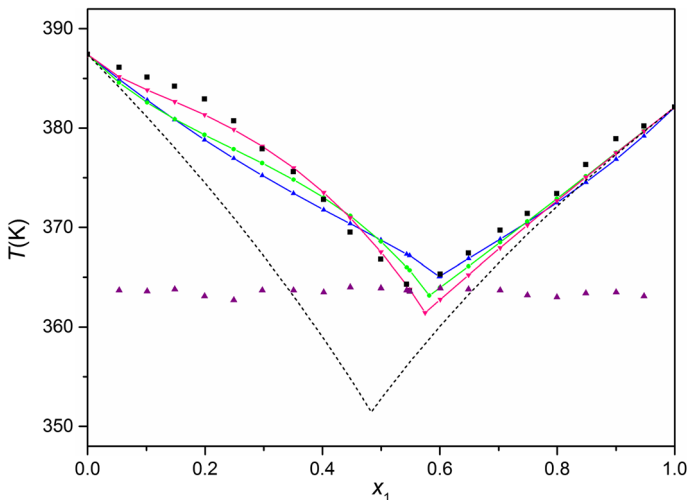| System	Parameters ($J \cdot mol^{-1}$)						Deviation σ^a (K)			
	Wilson $\Lambda_{12}-\Lambda_{11}$	Wilson $\Lambda_{21}-\Lambda_{22}$	NRTL $g_{12}-g_{11}$	NRTL $g_{21}-g_{22}$	UNIQUAC μ_{12}	UNIQUAC μ_{21}	Wilson	NRTL	UNIQUAC	Ideal
ENA(1) + ANA(2)	8252.36	−1486.96	−930.855	5923.68	615.515	410.969	1.25	1.80	2.07	7.63

^{a} According to Eq. 4

Fig. 4 Experimental and predicted SLE phase diagrams of ENA (1) + ANA (2): (■) liquidus; (▲) eutectic; (—▼—) Wilson; (—●—) NRTL; (—▲—) UNIQUAC; (- - -) Ideal

3.1.5 Excess Thermodynamic Functions

The excess thermodynamic functions, viz excess Gibbs energy, excess enthalpy and excess entropy of the mixture, are fundamental properties, which can provide a measure and type of the molecular interactions and the departure to ideal behavior.

The values of excess thermodynamic functions for the ENA (1) + ANA (2) system reported in Table S1 of the supplementary material are calculated using the temperature values obtained by the three semi-empirical models. Figure 5 shows these thermodynamic functions with respect to the mole fraction composition. All of the used models provide values highly comparable for a qualitative and quantitative analysis. Only the excess entropy values calculated by UNIQUAC equation present larger differences compared to those calculated by the two other models.

Inversely to what has been found often in the literature [28–30], where mathematical extremes had been found for those properties exactly at the eutectic composition, in this study it is not possible to observe a global maximum or minimum of those properties at the eutectic point. Nevertheless, the excess values at this particular mole fraction are close to the recorded minima or maxima, which can be most probably attributed to a consequence of the minimum temperature value at the eutectic.

As a rule, the sign and magnitude of the enthalpy and Gibbs energy of excess reproduce differences in the intensity of intermolecular attractions between pairs of dissimilar species on one hand, and pairs of like species on the other [31, 32]. As shown in Fig. 4, the studied system ENA (1) + ANA (2) shows a sensitive positive deviation to ideality. Both G^E/RT and H^E/RT are positive, which is a typical behavior for mixtures of an associative and a nonpolar compound, which it is not the case, even if ANA is for sure less polar than ENA. This positive deviation to ideality can be explained by the
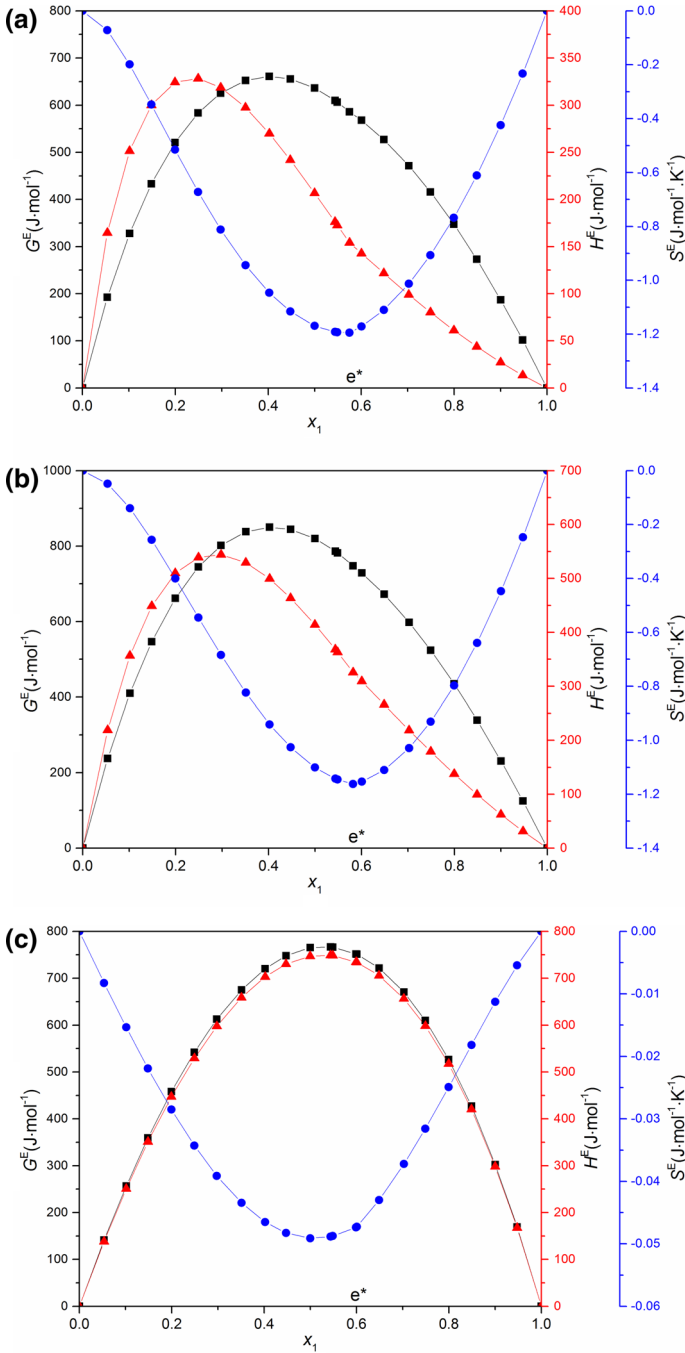
Fig. 5 Excess thermodynamic functions by (a) Wilson; (b) NRTL; (c) UNIQUAC: (■) G^E, (▲) H^E, (●) S^E for ENA (1)+ANA (2) system (e* is the eutectic composition)
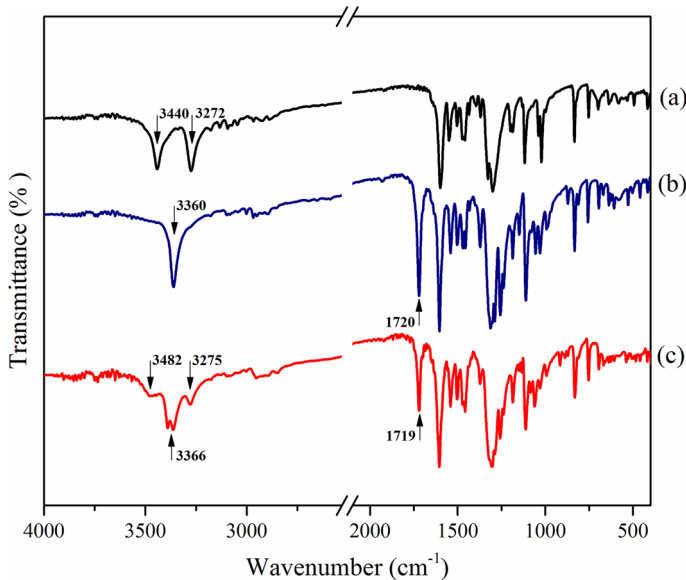
Fig. 6 FTIR spectra of (a) pure ENA, (b) pure ANA and (c) eutectic composition of the (ENA + ANA) system

presence of OH group (ENA) and the dominant effect of hydrogen bonding between ENA molecules (self-association), which will be shown later by FTIR analyses.

The structural contribution of the component fragment reproduces the sign and magnitude of excess entropy. Structure infringement involves a positive contribution to excess entropy and structure building a negative contribution to excess entropy [31]. From the negative values of the excess entropy obtained for the mixture ENA + ANA, it is likely that for that mixture a structure building takes place owing to gathering forces which makes clustering within the solution.

3.2 Molecular Interaction and Microstructure Studies of the Eutectic Mixtures

3.2.1 Fourier Transform Infrared Spectroscopy Analysis (FTIR)

FTIR studies are considered to provide information about molecular interactions between the mixture's components, especially at the eutectic composition. The FTIR spectra of pure components and the eutectic mixture under study are shown in Fig. 6. In general, hydrogen bonding to an X–H group results in a decrease in the X–H stretching frequency accompanied by a broadening and intensification of this band [33, 34]. Both OH and NH groups are found to exhibit highly characteristic changes with hydrogen bonding [34].

From FTIR spectrum of ENA (Fig. 6(a)), it can be revealed that in the solid state the ENA molecules are associated with each other by an intermolecular hydrogen bond. The stretching frequency of H-bonded –OH group appears at 3440 cm^{-1} which

is much lower than the stretching frequency of a non-hydrogen-bonded OH group, generally observed at higher frequencies, from 3580 up to 3670 cm^{-1} [34, 35], in particular when the molecular structure of the compound presents a steric hindrance [34] as is the case of ENA molecules. NH groups of the ENA have also involved hydrogen bonding since the NH stretching frequency (3272 cm^{-1}) is relatively lower than that of free NH group generally observed at higher frequencies (3300–3500 cm^{-1}) [34, 35].

The FTIR spectrum of the ANA (Fig. 6(b)) shows the inexistence of an inter- or intramolecular hydrogen bonding since the functional groups capable of giving rise to such binding are observed as free groups at FTIR stretching frequencies of 3360 cm^{-1} for NH and 1720 cm^{-1} for C=O [34, 35]. The absence of such characteristic bands in pure ANA reveals its inability to form intermolecular hydrogen bonding and predicts weak interactions between like ANA molecules that can be broken easily. The stretching frequencies of non-hydrogen bonded OH and NH groups obtained for similar compounds corroborate the pure component FTIR results reported above [36, 37].

The higher broadened frequency of the H-bonded –OH group at the eutectic mixture (Fig. 6(c)) indicates weak interaction due to the polarity difference between the two components. This promotes weak attractive forces between unlike molecules and reflects the dominant behavior of intermolecular hydrogen bonding in ENA, supported by the positive deviation to ideality obtained for the excess thermodynamic functions. Except that, we can clearly confirm that the eutectic spectrum gathers the totality of the characteristic frequencies of its respective pure components with no sensitive translation or shape modification of the characteristic frequencies, suggesting a weak molecular interaction between the two components in the mixture.

3.2.2 X-ray Diffraction Analysis (XRD)

The X-ray diffraction diagrams for the eutectic mixture superposed with those of the pure components are presented in Fig. 7. The Bragg angles, the inter-reticular distances and the Miller indices of the eutectic mixture, as well as those of the pure compounds, were evaluated by the EXPO 2014 software [38].

The results showed that the eutectic composition of the studied system crystallizes in a triclinic crystalline system, while its pure compounds ENA and ANA crystallize, both, in a monoclinic crystalline system. Moreover, from the XRD data of pure components and eutectic mixture of the studied system, it can be inferred that there is a difference in the interplanar distances (Tables S2-S4 of the Supplementary Materials) and the relative intensity. The variation in the relative intensity of reflections of pure components in the eutectic and the absence of some reflections of pure components in the eutectic suggest that the former, observed at 298.15 K, is not a simple mechanical mixture of two components [39] as it should be for a eutectic. Therefore, this change in the crystalline system of the eutectic should be explained by the formation of an intermediate solid below the eutectic, such as a peritectoid reaction.
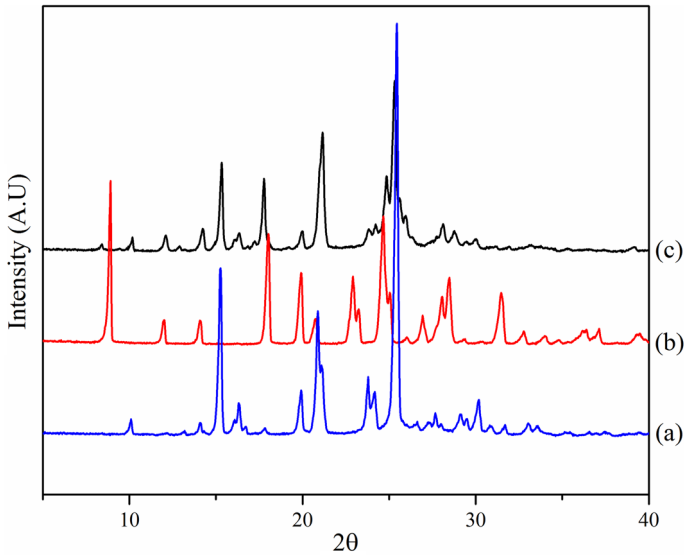
Fig. 7 X-ray diffractograms of (a) pure ENA, (b) pure ANA and (c) eutectic composition of the (ENA + ANA) system at $T = 289.15$ K

Fig. 8 Optical microscope microstructure at $50 \times$ magnification, (a) ENA, (b) ANA, (c) eutectic composition of (ENA + ANA) system

3.2.3 Optical Microscopy Microstructural Characterization

Microstructural studies are another important feature, which helps to understand the crystallization behavior of the materials. The microstructure of pure components and the eutectic composition are shown in Fig. 8. The microstructure of both pure ENA (a) and pure ANA (b) shows lamellar-type structure, whereas the eutectic mixture displays an irregular microstructure.

The microstructures and facet size are influenced by various factors. However, the microstructure of the eutectic mixtures could be predicted from the values of the fusion entropy. According to Hunt and Jackson [40], the type of growth from a binary melt can be predicted on the basis of roughness parameter α, defined as follows:

$$\alpha = {}^{\xi \Delta S_{fus}}\!/\!R = {}^{\xi \Delta H_{fus}}\!/\!RT_{fus} \tag{5}$$

Table 7 Roughness factor for the eutectic: ΔH_{eu}, α, ξ denote the eutectic fusion enthalpy, the roughness parameter and the crystallographic factor, respectively

System	ΔH_{eu} (kJ·mol^{-1})	α	
		$\xi = 0.5$	$\xi = 1.0$
ENA(1)+ANA (2)	17.3[a]	2.86	5.72

[a]Eutectic enthalpy of fusion uncertainty u is $u(\Delta H_{eu}) = 0.3$ kJ·mol^{-1}

where ξ is a geometrical coefficient often called as the crystallographic factor, depending upon the geometry of the molecules and has a value less than or equal to 1. The values of α (Table 7) were computed by substituting the ξ value by 0.5 and 1. It is reported that when the roughness parameter α is greater than 2, solidus–liquidus interfacial growth takes place with faceted morphology [40]. The values of α for the eutectic composition are found to be greater than 2, and thus, it possessed faceted morphology with irregular structure. The surface obtained is rather smooth, and the crystal develops with morphology side by side, with no interstices.

4 Conclusions

(Solid + liquid) phase equilibria for a binary mixture of nitrate ester-based propellants stabilizers have been investigated to predict its evolution and its thermodynamic behavior with respect to the temperature changes. The DSC technique is fairly satisfactory for the measurement of the SLE, with very satisfactory consistency quality factor. The studied system is a simple eutectic. The data concerning the SLE, in particular the eutectic composition of the systems, are of great importance in the stability evaluation of energetic materials.

The Wilson, NRTL and UNIQUAC models correlate accurately the binary SLE data and represent satisfactorily the solid–liquid phase diagram for the binary system. Inversely to what has been found often in the literature, excess properties at the eutectic composition do not present a minimum or maximum.

Microstructural and molecular interaction studies have shown the existence of some molecular interactions between the two components in the eutectic mixture, which crystallize in a different system from its respective pure compounds. Also, the eutectic displays an irregular microstructure what has been confirmed by the calculation of its roughness parameter.

This study will certainly contribute to a good understanding of the mixtures behavior of stabilizers and will be of great utility in the choice of storage conditions for ammunition. The results obtained will undoubtedly provide valuable information on the SLE of the stabilizers used in nitrate esters-based propellants. Thermodynamic and microstructural investigations carried out in this work allowed to verify that the eutectic compositions of binary mixtures of organic stabilizers can be introduced into the formulations of nitrate esters-based propellants.

References

1. J.P. Agrawal, *High Energy Materials: Propellants, Explosives and Pyrotechnics* (Wiley, Hoboken, 2010)
2. D. Trache, A.F. Tarchoun, J. Mater. Sci. **53**, 100 (2018)
3. S. Wilker, G. Heeb, B. Vogelsanger, J. Petržílek, J. Skládal, Propellants Explos. Pyrotech. **32**, 135 (2007)
4. M.A. Bohn, in *Nitrocellulose–Supply, Ageing and Characterization Meeting* (2007), pp. 24–25
5. D. Trache, K. Khimeche, A. Dahmani, Int. J. Thermophys. **34**, 226 (2013)
6. D. Trache, K. Khimeche, Fire Mater. **37**, 328 (2013)
7. W.P. de Klerk, Propellants Explos. Pyrotech. **40**, 388 (2015)
8. R. Baetens, B.P. Jelle, A. Gustavsen, Eng. Build. **42**, 1361 (2010)
9. P. Liu, J.-W. Hao, L.-P. Mo, Z.-H. Zhang, RSC Adv. **5**, 48675 (2015)
10. J.D. Gibson, (US Patent 5,387,295, 1995)
11. F. Zou, W. Zhuang, J. Wu, J. Zhou, Q. Liu, Y. Chen, J. Xie, C. Zhu, T. Guo, H. Ying, J. Chem. Thermodyn. **77**, 14 (2014)
12. D. Trache, K. Khimeche, R. Benelmir, A. Dahmani, Thermochim. Acta **565**, 8 (2013)
13. D. Wei, X. Zhang, H. Li, J. Chem. Thermodyn. **60**, 94 (2013)
14. M.H. Keshavarz, A.R. Akbarzadeh, R. Rahimi, M. Jafari, M. Pasandideh, R. Sadeghi, Fluid Phase Equilib. **427**, 46 (2016)
15. A. Jain, G. Yang, S.H. Yalkowsky, Ind. Eng. Chem. Res. **43**, 7618 (2004)
16. E. Baum, *Chemical Property Estimation: Theory and Application* (CRC Press, Boca Raton, 1997)
17. H. Gamsjäger, J.W. Lorimer, P. Scharlin, D.G. Shaw, Pure Appl. Chem. **80**, 233 (2008)
18. M. Matsuoka, R. Ozawa, J. Cryst. Growth **96**, 596 (1989)
19. J.W. Kang, V. Diky, R.D. Chirico, J.W. Magee, C.D. Muzny, A.F. Kazakov, K. Kroenlein, M. Frenkel, J. Chem. Eng. Data **59**, 2283 (2014)
20. D. Trache, K. Khimeche, M. Benziane, A. Dahmani, J. Therm. Anal. Calorim. **112**, 215 (2013)
21. U. Domańska, J. Łachwa, J. Chem. Thermodyn. **37**, 692 (2005)
22. J.M. Prausnitz, R.N. Lichtenthaler, E.G. de Azevedo, *Molecular Thermodynamics of Fluid-Phase Equilibria* (Pearson Education, Upper Saddle River, 1998)
23. R. Reddi, V.K. Satuluri, U. Rai, R. Rai, J. Therm. Anal. Calorim. **107**, 377 (2012)
24. R. Reddi, V. Kumar Satuluri, R. Rai, J. Therm. Anal. Calorim. **107**, 183 (2011)
25. A. Iddaoudi, N. Selhaoui, M.A. Amar, K. Mahdouk, A. Aharoune, L. Bouirden, J. Therm. Anal. Calorim. **110**, 923 (2012)
26. J.A. Nelder, R. Mead, Comput. J. **7**, 308 (1965)
27. T. Hofman, I. Nagata, Fluid Phase Equilib. **25**, 113 (1986)
28. P. Gupta, T. Agrawal, S.S. Das, N.B. Singh, J. Chem. Thermodyn. **48**, 291 (2012)
29. B. Sharma, N. Sharma, M. Rambal, Thermochim. Acta **206**, 71 (1992)
30. B. Sharma, R. Kant, R. Sharma, S. Tandon, Mater. Chem. Phys. **82**, 216 (2003)
31. S.M. Nayeem, Karbala Int. J. Mod. Sci. **3**, 176 (2017)
32. M. Okuniewski, K. Paduszyński, U. Domańska, J. Phys. Chem. **120**, 12928 (2016)
33. S.V. Latha, G.L. Flower, K.R. Reddy, C.N. Rao, A. Ratnakar, J. Solut. Chem. **46**, 305 (2017)
34. P. Larkin, *Infrared and Raman Spectroscopy: Principles and Spectral Interpretation* (Elsevier, Amsterdam, 2011)
35. G. Socrates, *Infrared and Raman Characteristic Group Frequencies: Tables and Charts* (Wiley, Hoboken, 2004)
36. S. Jeyavijayan, Indian J. Pure Appl. Phys. **43**, 269 (2016)
37. M.K. Trivedi, A. Branton, D. Trivedi, G. Nayak, K. Bairwa, S. Jana, Insights Anal. Electrochem. **1**, 5 (2015)
38. A. Altomare, N. Corriero, C. Cuocci, A. Falcicchio, A. Moliterni, R. Rizzi, Cryst. Res. Technol. **50**, 737 (2015)
39. N. Singh, B. Shukla, Cryst. Res. Technol. **20**, 345 (1985)
40. J. Hunt, K. Jackson, Trans. Metall. Soc. AIME **236**, 843 (1966)

Affiliations

Salim Chelouche[1] · **Djalal Trache**[1] · **Simão P. Pinho**[2,3] ·
Kamel Khimeche[1] · **Abderrahmane Mezroua**[1] · **Mokhtar Benziane**[4]

✉ Salim Chelouche
  salim.chelouche@gmail.com

✉ Djalal Trache
  djalaltrache@gmail.com

[1] UER Procédés Energétiques, Ecole Militaire Polytechnique, EMP, BP 17 Bordj-El-Bahri, Algiers, Algeria

[2] Associate Laboratory LSRE-LCM, Departamento de Tecnologia Química e Biológica, Instituto Politécnico de Bragança, Bragança, Portugal

[3] Mountain Research Center - CIMO, Polytechnic Institute of Bragança, 5301-857 Bragança, Portugal

[4] Ecole Supérieure du Matériel ESM, BP 188 Beau-Lieu, Algiers, Algeria